Department of Physics and Astronomy
University of Heidelberg

Bachelor Thesis in Physics
submitted by

Martin Kroesen

born in Solingen (Germany)

2014

Spectrum and Elliptic Flow of Direct Photons for a Space-Time Evolution from the Hydrokinetic Model

This Bachelor Thesis has been carried out by Martin Kroesen at the
Physikalisches Institut at the University of Heidelberg
under the supervision of
PD Dr. Klaus Reygers

Abstract – Measurements of Pb-Pb-collisions at $\sqrt{s_{NN}} = 2.76$ TeV at the LHC experiment ALICE show a larger direct photon production and elliptic flow at low transverse momentum than predicted. This is confirmed with the given data from a hydrokinetic model. Therefore photon rates are used to calculate the photon production and pQCD calculations are added. The measurements indicate a higher photon production at a later point of the expansion of the created fireball. Two possible additional photon sources are discussed. Bremsstrahlung in the hadron gas does not give the required contribution. A pseudo-critical enhancement of the photon production at the chemical freeze out from the quark gluon plasma to the hadron gas gives the required contribution.

Zusammenfassung – Messungen des Teilchenbeschleunigerexperiments ALICE von Blei-Blei-Kollisionen bei $\sqrt{s_{NN}} = 2.76$ TeV zeigen eine höhere Produktion direkter Photonen bei geringen Transversalimpulsen und einen höheren elliptischen Fluss als erwartet. Dies wird anhand des Hydrokinetischen Models überprüft und bestätigt. Dazu wird aus gegebenen Daten zur hydrokinetischen Beschreibung mit Hilfe von Photonraten die entsprechende Photonproduktion berechnet und pQCD Daten werden in die Rechnung integriert. Die Messwerte deuten auf eine erhöhte Photonproduktion zu einem späteren Zeitpunkt der Expansion des entstehenden Feuerballs hin. Zwei mögliche Produktionsquellen werden diskutiert. Dabei zeigt sich, dass Bremsstrahlung im Hadrongas keinen nennenswerten Beitrag liefert. Eine deutliche Erhöhung der Photonproduktion am Phasenübergang vom Quark-Gluon-Plasma zum Hadron-Gas führt zu den gemessenen Ergebnissen.

Note:

Numerical calculations were performed with "Root" [1].

In calculations of this thesis only natural units are used, which means $\hbar = c = k_B = 1$, where c is the speed of light, $\hbar$ is the reduced Planck constant, and k_B is the Boltzmann constant. The relations between the dimensions are given by: $[\text{length}] = [\text{time}] = [\text{energy}]^{-1} = [\text{mass}]^{-1}$.

Contents

1. Introduction

High-energy physics has established a detailed theory of the elementary particles and their fundamental interactions. This model is called Standard Model. It is the aim of ultra-relativistic heavy-ion physics to apply the Standard Model to dynamically evolving systems of finite size to understand the collective phenomena and microscopic properties of nuclear matter under conditions of extreme temperature and density [2].

The appearance of phase transitions involving elementary quantum fields is connected to the breaking of symmetries. Lattice calculations of quantum chromodynamics (QCD) predict a phase transition at a temperature of approximately 160 MeV [3]. At this temperature the nuclear matter is assumed to undergo a phase transition to a deconfined state of quarks and gluons, the quark-gluon plasma (QGP), and the quark masses are reduced to their small current ones.

Since the early 1980's, collisions of heavy atomic nuclei at as large energies as possible have been seen as the ideal way to probe these conditions of extremely high temperature and density [3]. There are two main conditions for the system to behave like bulk matter and not as a group of individual particles. The System must consist of a large number of particles and it needs to reach local equilibrium.

First indications for the creation of the QGP were observed at the Super Proton Synchrotron (SPS) at CERN and the Relativistic Heavy Ion Collider (RHIC) at the Brookhaven National Laboratory. The Large Hadron Collider (LHC) at CERN now offers the highest center-of-mass energies ever reached and should provide sufficient energy densities to create the QGP for a short time. The plasma is studied with the ALICE experiment, and also with CMS and ATLAS.

Photons interact only electromagnetically with matter. The coupling constant $\alpha_{em} \approx 1/137$ is much smaller then the coupling constant for strong interactions $\alpha_s \approx 0.3$ [4] at typical QGP temperatures. The photons produced during the QGP-phase leave the plasma without rescattering, because the mean free path λ is much larger than the lifetime of the fireball. The absence of rescattering makes the photon

an important tool for probing the space time development of the fireball. In this thesis the focus lies on direct photons, which include all photons except the decay photons.

While the fireball passes through several stages (thermalization, QGP phase and the hadronization), there are several sources for photon production contributing to the observables. Within this thesis the focus lies on the invariant yield (see section 3.1) and the anisotropic flow (see section 3.2). The anisotropic flow is a spatial anisotropy correlated with a momentum anisotropy.

The high slope in the ALICE direct photon yield measurements at $\sqrt{s_{NN}}$ could indicate a higher photon production in early stages of the created fireball. But in early stages of the expansion a collective flow is not expected to be formed yet. The measured direct photon elliptic flow for $1 < p_T < 3$ GeV is in the order of magnitude similar to the observed charged pion elliptic flow [5] (see figure 1.1). Similar results were published by the PHENIX collaboration [6]. Thus, a higher photon production in a later stage of the evolution is expected. It is the aim of this thesis to deliver contributions to the solution of this so called photon puzzle on the base of the well tested Hydrokinetic Model.

In chapter 2 the theoretical base is described, while chapter 3 deals with the observables for direct photon production. In chapter 4 "Models for Photon Production" the Hydrokinetic Model (HKM) as model of the flow on the one hand and the photon production on the other hand is explained. On this basis in chapter 5 "ALICE Data Modeling and Results" the measured data are compared with the model and discussed. Possible solutions of the photon puzzle are given in chapter 6.

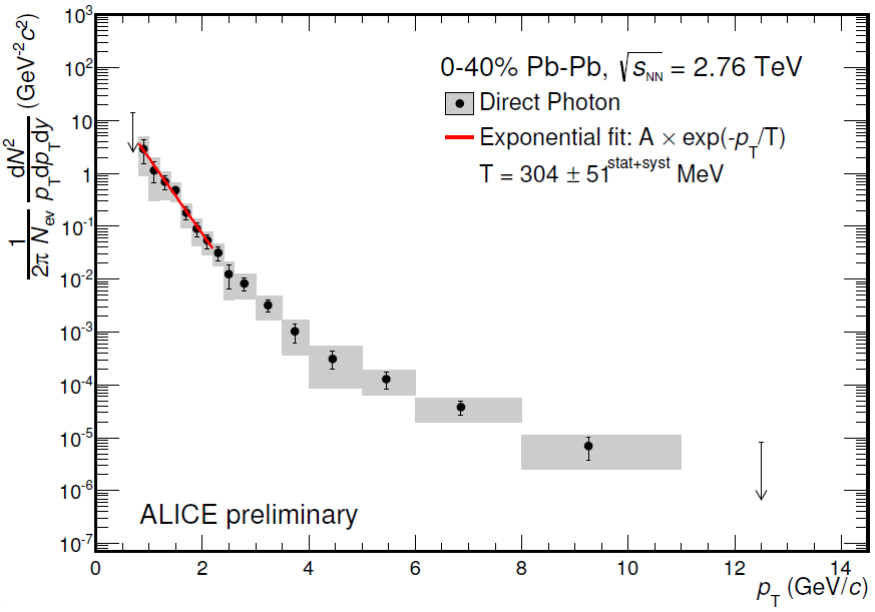

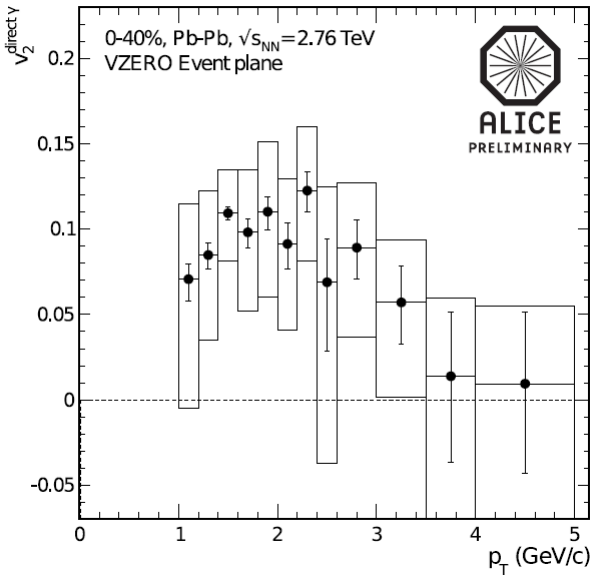

Figure 1.1:
Top: Direct photon yield with slope at low p_T [5]. Bottom: Elliptic flow from direct photons [5].

2. Theory

The aim of this chapter is to give a short overview over the theoretical background of this thesis.

2.1 QCD Fundamentals

Quantum chromodynamics (QCD) is the quantum field theory of the strong interaction, the interactions between color charged quarks and eight massless gluons. There are three different types of color charge, and anti-quarks carry the corresponding anti-color. Gluons also carry color charge and they do not only mediate the strong interaction between quarks, but also between the gluons themselves. A bound state of quarks and gluons will be colorless for an observer, they are called hadrons.

There exist the mesons, quark-antiquark pairs, and baryons, which consist of three quarks that are carrying different colors respectively anti-colors. The dynamic of quarks and gluons is described by the Lagrangian of quantum chromodynamics [4]:

$$\mathcal{L} = \sum_q \overline{\psi_q}\gamma_\mu \left(i\partial^\mu - g_s A_a^\mu \frac{\lambda_a}{2} \right) \psi_q - \sum_q m_q \overline{\psi_q}\psi_q - \frac{1}{4}\sum_a F_a^{\mu\nu} F_{\mu\nu,a} \tag{2.1}$$

ψ_q are the quark fields, g_s the strong coupling constant, A_q^μ the gluon fields, λ_a the Gell-Mann matrices. The gluon field strength tensor has the following form:

$$F_a^{\mu\nu} = \partial^\mu A_a^\nu - \partial^\nu A_a^\mu + g_s f_{abc} A_\mu^b A_\nu^c \tag{2.2}$$

In the early days of QCD the aim was the calculation of bound quark-antiquark pairs (mesons). The corresponding effective phenomenological, approximated potential of a quark-antiquark pair ($q\bar{q}$) is described by:

$$V(r) = -\frac{4}{3}\frac{\alpha_s(r)}{r} + \kappa \cdot r \tag{2.3}$$

Here, α_s is the strong coupling constant and κ is the string tension. The second term increases linearly and is linked to the concept of confinement. This is the reason for quark systems being colorless for an observer. The first term is, aside from the different coupling constant, similar to the Coulomb potential.

One very important point of QCD is the running coupling constant α_s, it depends on r, respectively the invariant squared momentum transfer Q^2:

$$\alpha_s(Q^2) = \frac{12 \cdot \pi}{(33 - 2n_f) \cdot (Q^2/\Lambda^2)} \tag{2.4}$$

n_f is the number of quark flavors and Λ the QCD scaling parameter. Λ is measured to be approximately 200 MeV. This equation only takes effect if $Q^2 \gg \Lambda^2$.

While in normal matter quarks are confined, in the quark-gluon plasma (QGP) quarks are deconfined. This phase is thought to consist of asymptotically free quarks and gluons.

2.2 Heavy-ion Collisions

It is expected that the universe has been in a state of very high temperature and density in the first fraction of a second. In this state the strongly interacting quarks and gluons were asymptotically free and in a deconfined phase of matter, the so called quark-gluon plasma (QGP). In the description of the Big Bang, this plasma cools into confined hadrons after a short time. In this context the QGP behaves like a distinct state of matter. To work with the QGP and probe its conditions, it should not behave like individual elementary particles or a group of those, but like matter [3].

To probe the QGP on earth, we need such a high temperature, so that the characteristic thermodynamic parameters like energy-density, temperature, entropy-density and pressure are sufficiently high to constitute the phase transition. To reach a local thermodynamic equilibrium the inverse rate of interactions must be significantly larger than the system's lifetime. Simple collisions of electrons or protons do not produce these conditions. But it is known that high energy collisions of heavy atomic nuclei can produce the conditions to create a fireball of interacting quarks and gluons. Figure 2.1 shows the schematic phase diagram of QCD with points that were

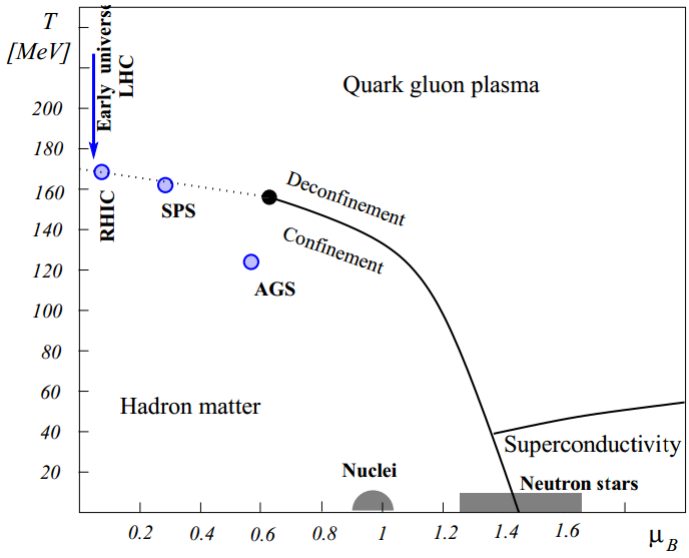

Figure 2.1: Schematic phase diagram of QCD in the plane of temperature T and baryon chemical potential μ_B with points that were tested in heavy ion experiments so far [7].

tested in heavy-ion experiments so far. Thus the collisions of heavy-ions at very high energies are found to be the ideal way for the research of the QGP under lab conditions on earth.

The Large Hadron Collider (LHC) provides Pb-Pb-collisions with a center-of-mass collision energy of 2.76 TeV per nucleon-nucleon pair.

2.3 Space Time Evolution of the Fireball

After the collision of the heavy-ions a state of very high energy, pressure and density is established. We cannot describe the process of formation itself. We start the description at a point a very short time after the collision of the ions. The process can be described by four stages [9].

In the pre-equilibrium stage the process is dominated by parton-parton hard scattering and can be modeled by perturbative QCD (pQCD). The lifetime of this phase is predicted to be about less 1 fm [10, 11].

After this very short phase the QGP is established (see figure 2.2). This phase is dominated by parton-parton, string-string interactions and thermal equilibrium.

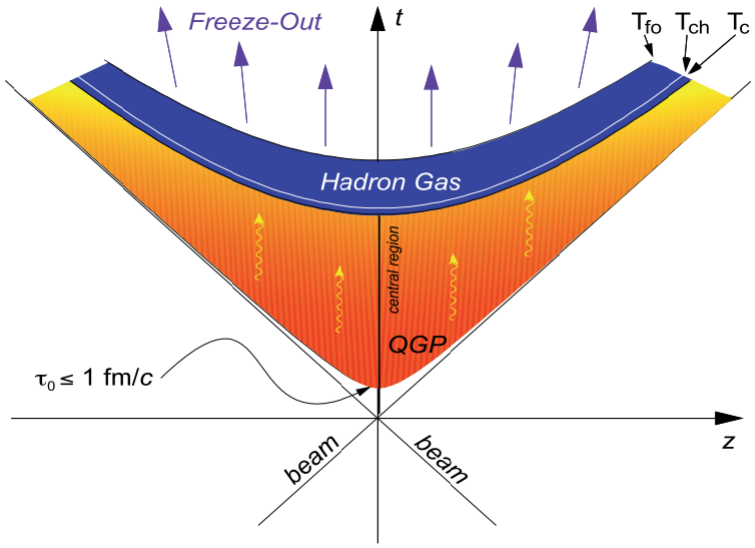

Figure 2.2: Light cone diagram of the evolution of ultra relativistic heavy ion collisions [8].

It behaves like an almost ideal fluid. A rough description can be found in "Highly relativistic nucleus-nucleus collisions: The central rapidity region" by J. D. Bjorken [10]. The plasma expands while the temperature and the corresponding energy-density are decreasing. The energy density is expected to be around 3-5 GeV/fm^3.

When the local temperature reaches approximately the critical temperature T_c, quarks and gluons are being confined. In this mixed phase, a soft crossover, escaping particles are produced. The critical temperature is expected to be around 160 MeV.

In the last phase, the hadronic phase, a collective expansion via hadron-hadron interactions decreases the temperature. At the hadron freeze-out temperature T_f, the non-interacting particles stream out of the medium into the detectors.

The space time evolution of the QGP can only be deduced by observing the escaping particles and the direct photons (see section direct photons). Thus a model for the QGP-expansion and a model for photon production from the plasma is needed. In this context the base is a Hydrokinetic Model describing the space time evolution.

3. Direct Photon Observables

Direct photons are those photons that directly emerge from a particle collision within the fireball. The measurement of direct photons plays an important role in probing the properties of the QGP. Direct photons give an interesting view into the interior (early) part of the QGP and other states of the evolution since they are produced continuously during the expansion. This distinguishes them from the produced hadrons, which are the result of the freeze-out, and from decay photons.

There are different processes which produce direct photons [12]. One possibility is hard scatterings of incoming partons. The jet fragmentation process can also constitute direct photons after initial hard scattering. These processes can be calculated with pQCD. Scattering between quarks and gluons in the QGP and scattering between hadrons in the hadron gas are also important direct photon sources. These processes are thermal and give rise to an interpretation of the spectra as effective temperature.

In this chapter, the two observables direct photon yield and anisotropic flow, especially the elliptic flow, are discussed. In the following chapters these observables will be used for a qualitative analysis of the direct photons.

3.1 Invariant Photon Yield

For basic kinematics as background knowledge look at A.1 in the appendix. We are interested in the observable

$$\frac{1}{L_{int}} \frac{d^3N}{dp^3} \tag{3.1}$$

of the photons. N is the number of particles, p the momentum and L_{int} is the integrated luminosity. In contrast to d^3p the phase space element $\frac{d^3p}{E}$ is Lorentz invariant. So with E' and p' being the energy, respectively the momentum, in another coordinate frame, the following relation is given:

$$\frac{d^3p}{E} = \frac{d^3p'}{E'} \tag{3.2}$$

Thus it makes sense to define a corresponding observable, the Lorentz invariant cross section

$$\frac{1}{L_{int}} E\frac{d^3N}{dp^3} = \frac{1}{N_{evt,tot}} E\frac{d^3N}{dp^3}\sigma_{tot} \tag{3.3}$$

where $N_{evt,tot}$ is the total number of events and σ_{tot} the total cross section. The invariant photon yield is now defined by

$$E\frac{d^3n}{dp^3} = \frac{1}{N_{evt,tot}} E\frac{d^3N}{dp^3} \tag{3.4}$$

The invariant photon yield can be calculated from convolving the photon rates $f(E,T) := q_0 \frac{d^3R}{dp^3}$ with the space-time evolution of the emitting medium [13]:

$$E\frac{d^3n}{dp^3} = \int \tau d\tau dY dx dy f(p\cdot u, T) \tag{3.5}$$

Note: T is the temperature in the rest frame and $d^4X = dt\ dx\ dy\ dz = \tau d\tau\ dY\ dx\ dy$. The scalar $p\cdot u = p_\mu u^\mu$ is the Lorentz invariant product of the photon four-momentum p^μ and the four-velocity $u^\mu = \gamma(1, \beta_x, \beta_y, \beta_z)$ of the cell from which the photon is emitted. In the rest frame of the cell $p \cdot u = E$ and thus the rate f is calculated by $f(p \cdot u, T)$.

The integration limits over Y are given by the beam rapidity of the projectile:

$$Y_{max} = y_{max} = \frac{1}{2}\ln\frac{E+p_z}{E-p_z} = \frac{1}{2}\ln\frac{(E+p_z)^2}{E^2-p_z^2} = \ln\frac{(E+p_z)}{m_N} \approx \frac{\sqrt{s}}{m_N} \tag{3.6}$$

To calculate the invariant yield, we need a model which describes the flow of the cell, in our case the Hydrokinetic Model, and a model for the photon production, to calculate the rate $f(p \cdot u, T)$ (section 4.2 "Thermal Photon Rates from the Hadron Gas and Quark-Gluon Plasma").

3.2 Anisotropic Flow

Flow signals the presence of multiple interactions between the constituents of the medium created in collisions [14]. A larger magnitude of flow is correlated to an increasing number of interactions. The most direct evidence of flow comes from the observation of anisotropic flow, which is the anisotropy in particle momentum distributions correlated to the reaction plane. The reaction plane is defined by the

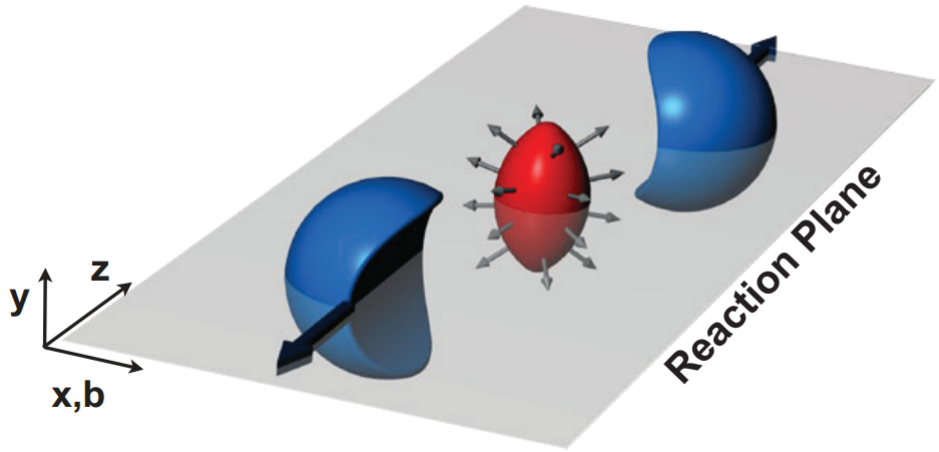

Figure 3.1: After a non-central collision of two nuclei the spatial anisotropy with respect to the x-z plan (reaction plane) translates into a momentum anisotropy of the produced particles (anisotropic flow) [14].

impact parameter and the z-direction. It is convenient to describe the invariant yield by its Fourier expansion around the reaction plane (figure 3.1)

$$E\frac{d^3N}{dp^3} = \frac{1}{2\pi}\frac{d^2N}{p_T dp_T dy}\left(1 + 2\sum_{n=1}^{\infty} v_n \cos(n(\phi - \psi_{RP}))\right). \tag{3.7}$$

E is the energy of the particle, p the momentum, p_T the transverse momentum, ϕ the azimuthal angle, y the rapidity and ψ_{RP} the reaction plane. Because of the reflection symmetry with respect to the reaction plane the sine terms vanish. The Fourier coefficients are depending on p_T and y. They are given by:

$$v_n(p_T, y) = \langle \cos[n(\phi - \psi_{RP})] \rangle \tag{3.8}$$

The angular brackets denote an average over the particles. The coefficient v_1 is known as direct flow while v_2 is known as elliptic flow.

v_n is related to the eccentricity and the radial flow velocity [15].

4. Models for Photon Production

To describe the photon production from the fireball we need two model parts. The first part describes the dynamics of the fluid within the fireball, the second part describes the distribution of photon rates of emerging direct photons.

In our case the dynamics of the fluid are described by the so-called Hydrokinetic Model (HKM). Concrete data sets describing the space-time evolution of the flow velocity and temperature are provided by Yuri Sinyukov and they are used as a black-box in this thesis.

The second model part describes the thermal photon emission rates from the quark-gluon plasma and the hadron gas.

First a motivation for the use of the HKM is given. A combined hydrokinetic approach which incorporates a hydrodynamical expansion of the fireball and their dynamical decoupling by escape probabilities describes the space time distribution of the flow [17].

On the base of such models predictions for the particle yield in central Pb-Pb collisions were made [18][19]. Figure 4.1 shows the transverse momentum distributions of the sum of positive and negative particles [16]. As pointed out in this publication, HKM yields a good description of the data. Because the description of hadronic final states using HKM works well, it seems reasonable to choose this model as a basis to study the production of direct photons.

4.1 Description of the Hydrokinetic Model

The history of the QGP models has a long tradition. Early hydrodynamic models for example, were presented by Bjorken [10]. An overview of the main characteristics is given by Ollitrault [20] and some properties are given in the appendix of this thesis.

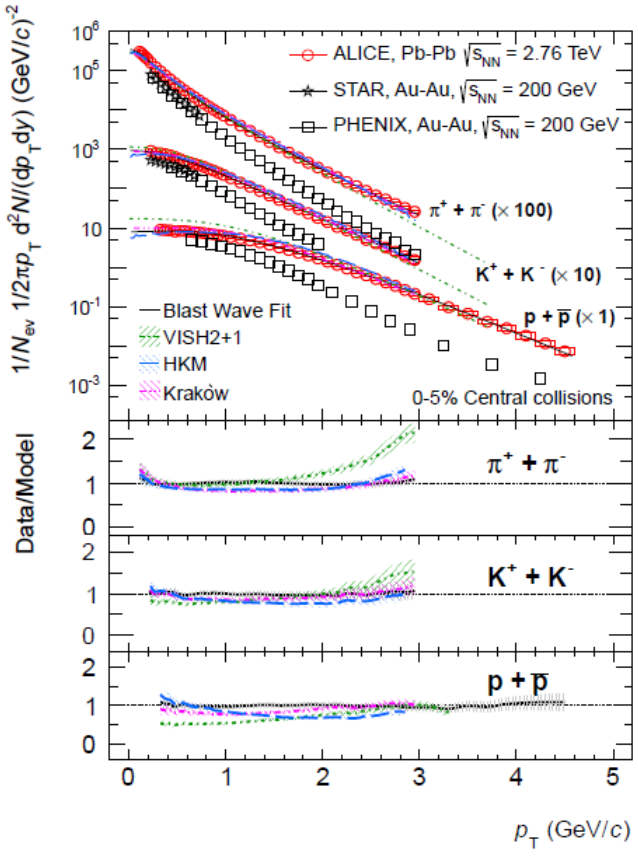

Figure 4.1: Transverse momentum distributions of the sum of positive and negative particles [16].

Such hydrodynamic models successfully describe basic features of high energy collisions. In these models a state of equilibrium shortly after the collision is assumed. The QGP phase is given by the stress-energy tensor and the equation of state (EOS).

Since the HKM is used as a black-box in this thesis, only a small overview can be given. Figure 4.2 shows the evolution of the fireball in the HKM. It incorporates a description of the pre-thermal phase [11] [22], to assess the initial conditions for hydrodynamics. To obtain these conditions for $\tau \gtrsim 1$ fm one needs to match the very early initial stage of the nuclei collision, when the hydrodynamic approximation is outside the regime of its validity. The corresponding evolutional equations are then written as [11]

$$\partial_\mu[(1 - P(x))T^{\mu\nu}_{hyd}(x)] = -T^{\mu\nu}_{pQCD}\partial_\mu P(x). \tag{4.1}$$

In this case $P(x)$ is a probability function (continuous switch) that transforms $T^{\mu\nu}_{pQCD}$ into $T^{\mu\nu}_{hyd}$. With the help of this equation the initial conditions of the QGP phase,

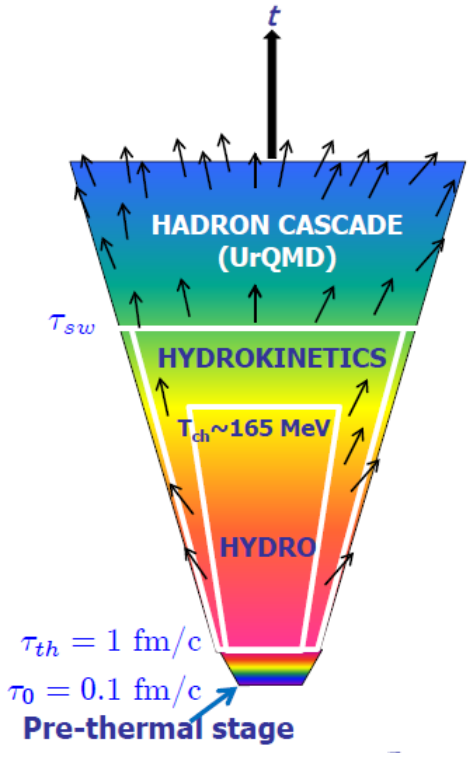

Figure 4.2: Different stages in the description of the HKM. The hadron cascade is not relevant in our case [21].

which are dominated by $\partial_\mu T^{\mu\nu}_{hyd} = 0$ and the EOS, are calculated.

In addition to the calculation of reasonable initial conditions, an approach for the freeze-out, that means a dynamical description of the decoupling in space time, is needed, since a sharp freeze-out is however a rather rough approximation.

An early description of this process in the context of hydrokinetics is given by [23]. The hydro-kinetic formalism for heavy ion collision is described in [17]. It includes a model of hadronic emission that describes the evolution of a hydrodynamically expanding system undergoing a phase transition. The complete algorithm provides the evaluation of an emission function based on escape probabilities with account for deviations of distribution functions f(x,p) from local equilibrium [24, 25, 19]. As above a soft switch (escape probability) is used, to transform the QGP into the hadron gas, so we get a soft decoupling and hadronization.

4.2 Thermal Photon Rates from the Hadron Gas and Quark-Gluon Plasma

The main source of direct photons (figure 4.3) in the fireball are photons emitted from the quark-gluon plasma at temperatures above T_C and hadronically produced thermal photons from below the phase transition. In our case the description of the former (QGP-rates) is taken from Arnold, Moore and Yaffe (AMY) [26] and the latter (HG-Rates) is from Turbide, Rapp and Gale [27].

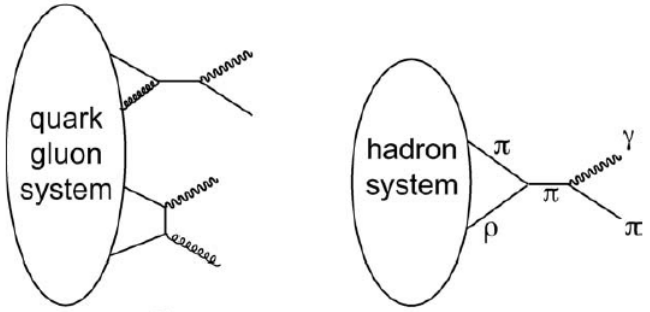

Figure 4.3: Direct photons from HG and QGP [12].

To calculate the observables (see section 3.1 / 3.2 for details) like the QGP photon-rate $E_\gamma \frac{dN_\gamma}{dp^3}$ we need the rate $f(E,T) := q_0 \frac{d^3R}{dp^3}$.

The photon emission rate of an equilibrated QCD plasma at high temperature with zero chemical potential has been computed in detail by AMY [26]. The results from AMY are used in this thesis. In the special case of QCD with $d_F = N_C = 3$ and $C_F = 4/3$ the equation for the photon emission rates $f(E,T)$ can be written as:

$$f(E,T) = \sum_{i=1}^{N_f} q_i^2 \frac{\alpha_{em}\alpha_s}{\pi^2} T^2 \frac{1}{e^x + 1} C_{tot}(x) \tag{4.2}$$

x is defined by $x := \frac{E}{T}$ and C_{tot} is given by

$$C_{tot}(x) = \ln \frac{\sqrt{3}}{g_s} + \frac{1}{2}\ln(2x) + C_{2\leftrightarrow 2}(x) + C_{brems}(x) + C_{annih}(x). \tag{4.3}$$

The rate has been calculated to leading order in α_{em} and the QCD-coupling $g_s^2(T) = 4\pi\alpha_s$ which should always be understood as defined at a scale of order of the tem-

perature.

The rate $f(E,T)$ is dominated by the Fermi distribution function $\frac{1}{e^x+1} \approx e^{-x}$, which leads to the rough $e^{-E_\gamma/T}$ behavior of the QGP photon rate.

The leading logarithmic order contribution is generated by $2 \leftrightarrow 2$ particle processes. The $C_{2\leftrightarrow 2}$-term represents the non logarithmic $2 \leftrightarrow 2$ particle processes. The rate of photon production by bremsstrahlung and inelastic pair annihilation is given by C_{brems} respectively C_{annih}.

From AMY [26] we get the approximate, phenomenological fits:

$$C_{2\leftrightarrow 2} \approx \frac{0.041}{x} - 0.3615 + 1.01e^{-1.35x} \tag{4.4}$$

and

$$C_{brems} + C_{annih} \approx \sqrt{1+\frac{1}{6}N_f}\left[\frac{0.548\ln(12.28+x^{-1})}{x^{3/2}} + \frac{0.133x}{\sqrt{1+x/16.27}}\right] \tag{4.5}$$

The above equations are useful in the context of the QGP at temperatures $T > T_c$ and were used in our calculations.

The thermal emission of photons from hot and dense strongly interacting matter at temperatures close to the phase transition to the QGP were calculated by Turbide, Rapp and Gale [27]. Useful parametrizations were given in the appendix of the paper and are used in our context. The parametrizations are of the form

$$f(E,T) = A\exp(\frac{B}{(2ET)^C} - D\frac{E}{T}). \tag{4.6}$$

The parametrizations from [27], which are more detailed, are used at $T <= T_c$, thus we have a sharp transition between those rates at T_c.

4.3 Blueshift

The invariant photon yield is given by (as described above):

$$E\frac{d^3n}{dp^3} = \int \tau d\tau dY dx dy f(p \cdot u, T) \tag{4.7}$$

In this section, we want to discuss the impact of the $p \cdot u$ term. In the case of massless photons, p^μ is given by

$$p^\mu = p_T \cdot (1, \cos(\phi), \sin(\phi), 0) \tag{4.8}$$

and $p \cdot u$ is expressed by

$$p_\mu u^\mu = p_T(u_0 - u_1 \cos(\phi) - u_2 \sin(\phi)). \tag{4.9}$$

For simplicity we look at a fluid with $u_2 = 0$ and $Y = 0$ and a photon with $\phi = 0$. In this case u^μ is given by

$$u^\mu = (cosh(\rho), sinh(\rho), 0, 0) = (\gamma_{flow}, \beta_{flow}\gamma_{flow}, 0, 0) \tag{4.10}$$

and we can conclude

$$p_\mu u^\mu = p_T(\frac{1}{\sqrt{1-\beta_{flow}^2}} - \frac{\beta_{flow}}{\sqrt{1-\beta_{flow}^2}}) = p_T\sqrt{\frac{1-\beta_{flow}}{1+\beta_{flow}}}. \tag{4.11}$$

Since $f(p \cdot u, T)$ is described by

$$\sum_{i=1}^{N_f} q_i^2 \frac{\alpha_{em}\alpha_s}{\pi^2} T^2 \frac{1}{e^x + 1} C_{tot}(x) \tag{4.12}$$

it is reasonable to write

$$x = \frac{p_T\sqrt{\frac{1-\beta_{flow}}{1+\beta_{flow}}}}{T} = \frac{p_T}{T\sqrt{\frac{1+\beta_{flow}}{1-\beta_{flow}}}} \tag{4.13}$$

and we define

$$T_{slope} = T\sqrt{\frac{1+\beta_{flow}}{1-\beta_{flow}}}. \tag{4.14}$$

We interpret T_{slope} as effective blueshifted temperature. If we take $\beta_{flow} = 0.6$, then $\sqrt{\frac{1+\beta_{flow}}{1-\beta_{flow}}} = 2$, thus the large slope at low p_T in the invariant yield can be partially explained by photons emitted with sufficient high β_{flow}. For more details see [28].

4.4 pQCD Photons

In the last sections thermal photon production in the QGP and HG (Hadron Gas) phase has been described. However, direct photons of other kinds can also play an important role. The full palette of opportunities has been explored in a paper from Stankus [12]. Hard scattering of incoming partons can create direct photons.

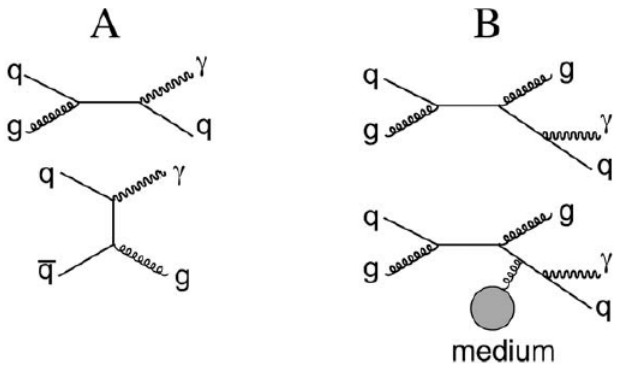

Figure 4.4: Two types of processes emitting pQCD photons [12].

At high p_T these processes can be described by perturbative QCD (pQCD) and their rate can be calculated in this framework, thus they are called pQCD-Photons. Two perturbative QCD diagramms that produce final-state photons at lowest order are shown in 4.4 Panel A. As part of the jet fragmentation process a quark can also radiate photons after its initial hard scattering process (upper diagram of Panel B). Photons from those in Panel B are always accompanied by hadrons and are termed fragmentation photons while a Photon like Panel A is a single direct photon.

5. ALICE Data Modeling and Results

In this chapter spectrum and elliptic flow of direct photons for the space-time evolution from the Hydrokinetic Model are compared to the ALICE preliminary data at 2.76 TeV center-of-mass energy with a centrality of 0-40%.

In the first part the raw data is briefly shown and in the following the pQCD photons are added.

5.1 HKM Data - Only Thermal Photons

On the basis of existing HKM-data (discrete data sets) by Yuri Sinyukov describing the flow and temperature as a function of the space-time, the direct photon yield and the elliptic flow v_2 are calculated as a function of p_T.

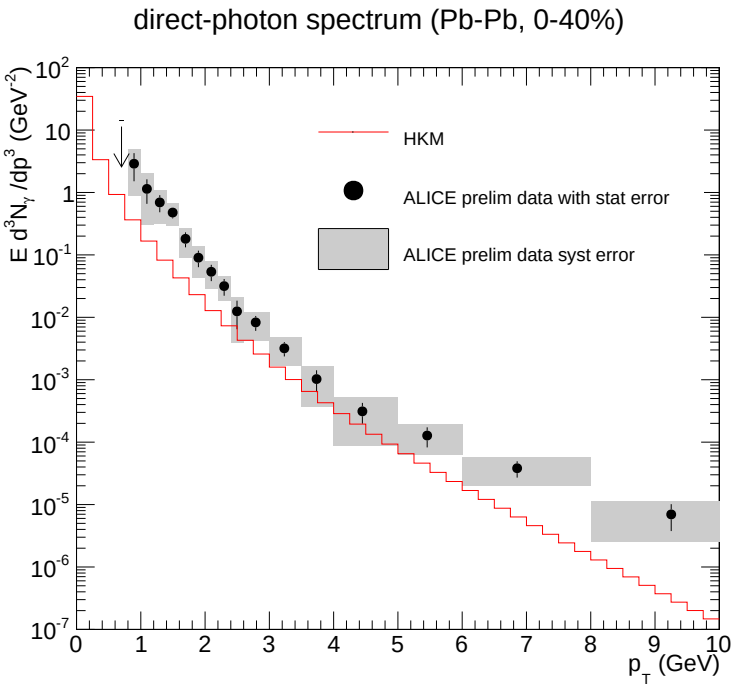

Figure 5.1: Comparision of HKM direct photon yield with ALICE data.

The blueshift is implicitly included in the calculations. A sharp crossover from the

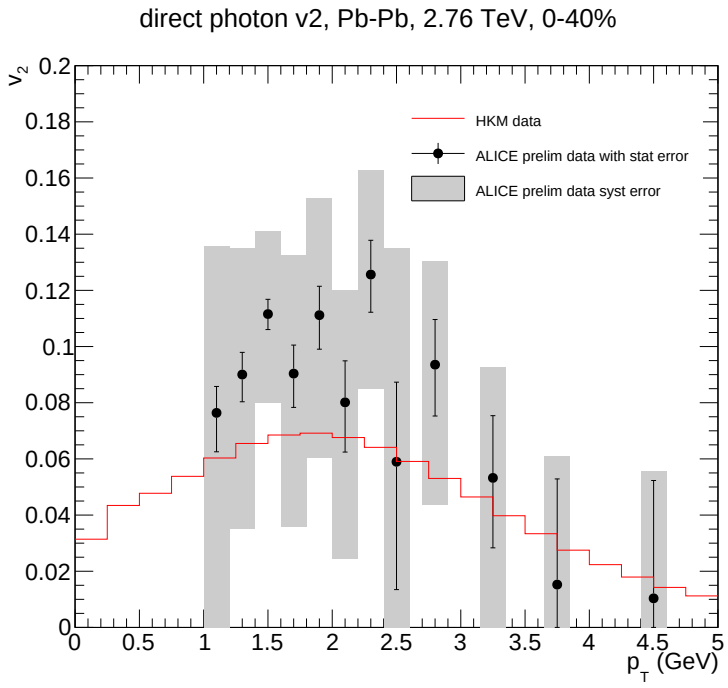

Figure 5.2: Comparison of HKM v_2 calculation with ALICE data.

parametrization of the QGP rates to the HG rates at $T_c = 160$ MeV is implemented in our calculation for simplicity, even though it is in contrast to the soft crossover of the HKM.

Figure 5.1 shows the direct photon yield while figure 5.2 shows the p_T-dependency of v_2.

Since $v_2(p_T \to 0) = 0$ should apply, this behavior has been tested for a very small binning.

The model based pure HKM direct photon yield is, as expected, low. The rough shape is dominated by the factor $e^{-\frac{p_T}{T_{eff}}}$. A blueshift is visible at low p_T, the slope increases with smaller p_T. At large p_T some physical processes seem to be missing. The deviation of model based data for small and high p_T is large and underestimating the measurements.

Figure 5.2 shows $v_2(p_T)$. The maximum of v_2 is at $p_T \approx 2$GeV with $v_2 \approx 0.07$. The measured values are underestimated although the rough shape of the measured data corresponds to the calculated spectra.

As an interim result it can be stated, that additional photon sources are needed for a better description of the measured data. It is expected that pQCD corrections become relevant at high p_T. So our first expectation is that such corrections will solve the deviation only at that region.

5.2 pQCD Correction

The pQCD data used in this thesis were calculated by Werner Vogelsang for proton-proton collisions [29]. For lead-lead collisions these have to be scaled with a factor

$$\langle T_{AA} \rangle = \frac{\langle N_{coll} \rangle}{\sigma_{inel,NN}} \tag{5.1}$$

corresponding to the mean value of the number of inelastic nucleus-nucleus collisions $\langle N_{coll} \rangle = 826.46$ and the nucleus-nucleus inelastic cross section $\sigma_{inel,NN} = 64\text{mb}$.

The provided discrete data were difficult manageable in our context, thus we need a continuous parametrization. We made a reasonable fit with the function

$$\frac{1}{2\pi p_T}\frac{d^2N}{dp_T dy} = \frac{A}{2\pi}\frac{(n-1)(n-2)}{nC[nC+m(n-2)]}\left(1+\frac{\sqrt{p_T^2+m^2}-m}{nC}\right)^{-n}. \tag{5.2}$$

Apparently it is suitable (see figure 5.3). The parametrization is from [30] (equation 3 in the appendix). At small p_T below 2 GeV the data is extrapolated due to reasons of practical calculation. In this region the influence of the pQCD data is very low.

To recalculate the elliptic flow, we make the reasonable assumption that $v_{2,pQCD} = 0$, because pQCD photons are presumably mainly emitted at a very early stage in the evolution of the fireball. The pQCD photons are emited from scattering of initial partons.

We can calculate the $v_{2,direct}$

$$v_{2,direct} = f * v_{2,therm} \tag{5.3}$$

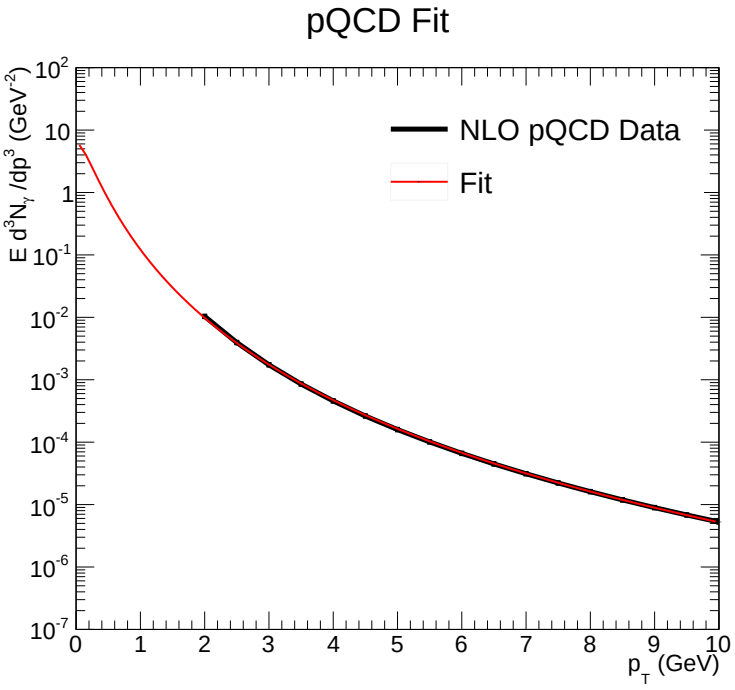

Figure 5.3: Black line: pQCD calculation from [29]. Red line: Fit with eq 5.2.

with the normalization $f = \frac{N_{therm}}{N_{therm}+N_{pQCD}}$.

Adding the HKM data and the pQCD contribution we obtain figures 5.4 and 5.5.

At $p_T > 3$ GeV the invariant yield is now described well, but apparently at low p_T we seem to need additional processes. Since $f = \frac{N_{therm}}{N_{therm}+N_{pQCD}} < 1$, we expect a smaller v_2 when including pQCD contributions. As shown in figure 5.5 this is confirmed.

Our interim result is, that pQCD corrections deliver no solution for v_2 but high p_T-spectra are well described. Although the calculation of the photon rates from the HKM incorporates the blue shift, the low p_T data is not well described. The high slope of the measured data could be due to a higher photon production in the QGP. Since we know that in the early stages of the expansion of the fireball, the collective flow has not build up yet, we expect a low v_2. The photon rates from the HKM also give rise to a low v_2. An explanation for the high measured v_2 could be additional photon sources at a later stage of the expansion, when the collective flow is predicted to be formed. We call this problem the "Photon Puzzle". Two possible solutions are presented in the next chapter 6.

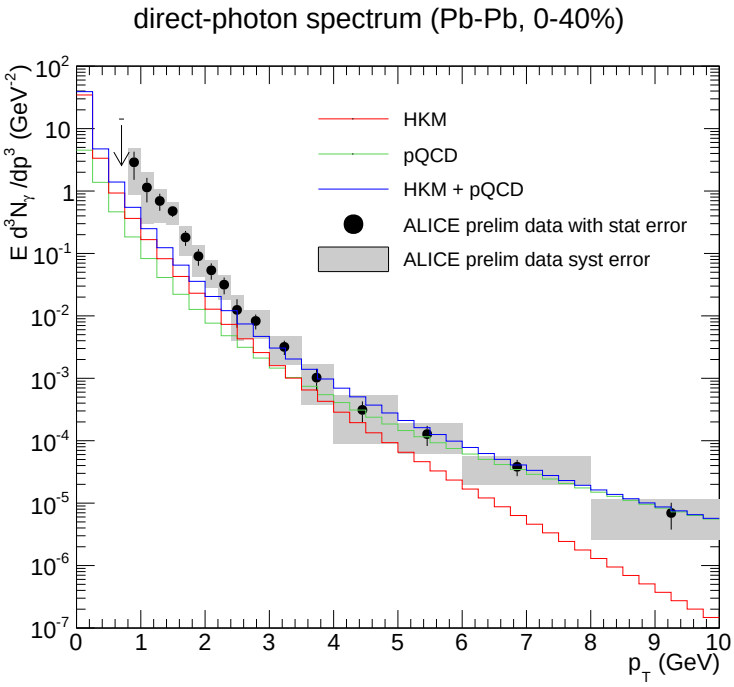

Figure 5.4: Model includes HKM and pQCD data. The experimental data are well described at high p_T.

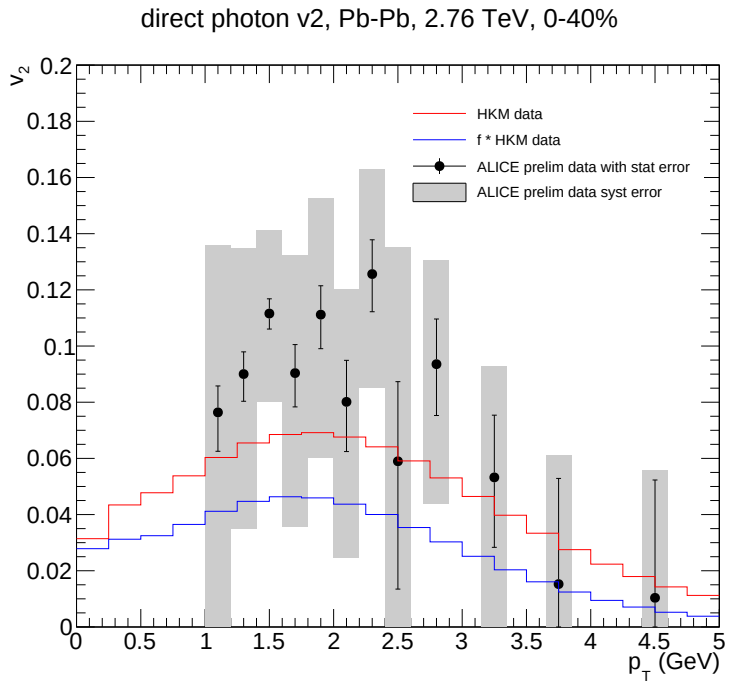

Figure 5.5: Photons calculated from the HKM show a smaller v_2 than the measured data.

6. Two Possible Solutions to the Direct Photon Puzzle

In this section, the effect of meson-meson and meson-baryon bremsstrahlung and a pseudo-critical enhancement inspired by [31] is discussed. Both sources of direct photons emerge from a later stage of the expansion and so they are predicted to give a higher contribution to the elliptic flow.

6.1 Bremsstrahlung

Linnyk et al. [32] had proposed that apart from partonic production channels the direct photon yield and primary the strong v_2 might be due to hadronic photon sources such as meson-meson bremsstrahlung.

Thus including meson-meson and meson-baryon bremsstrahlung may give a hint to the photon puzzle. A parametrization for the bremsstrahlung is provided by O. Linnyk et al. [33].

For $\pi + \pi \rightarrow \pi + \pi + \gamma$ the rate has the following form:

$$f_{brems}(x,T) = ln(ax+1) \cdot b \cdot exp\left(-\frac{x}{c}\right) + d \cdot exp\left(-\frac{x}{e}\right) \tag{6.1}$$

with the parameters a, b, c, d, e given in table 6.1. The result is in GeV^{-2} fm^{-4}.

The total meson-meson and meson-baryon bremsstrahlung is approximately obtained

T [MeV]	a	b	c	d	e
140	4	0.0025	0.1	0.008	0.05
150	5	0.004	0.105	0.015	0.05
160	5	0.007	0.11	0.025	0.05
170	5	0.01	0.116	0.04	0.05
180	5	0.015	0.125	0.06	0.05

Table 6.1: Parameters used in equation 6.1.

by multiplying the result with 4 [33]. To make the data usable for our purpose the data is interpolated with a spline.

From figure 6.1 it becomes obvious that the bremsstrahlung only gives a small contribution to the invariant yield at low p_T and there, the yield is systematically underestimated. Nevertheless the slope is nearly the same as the slope from the photon yield at low p_T. The low p_T problem remains unsolved.

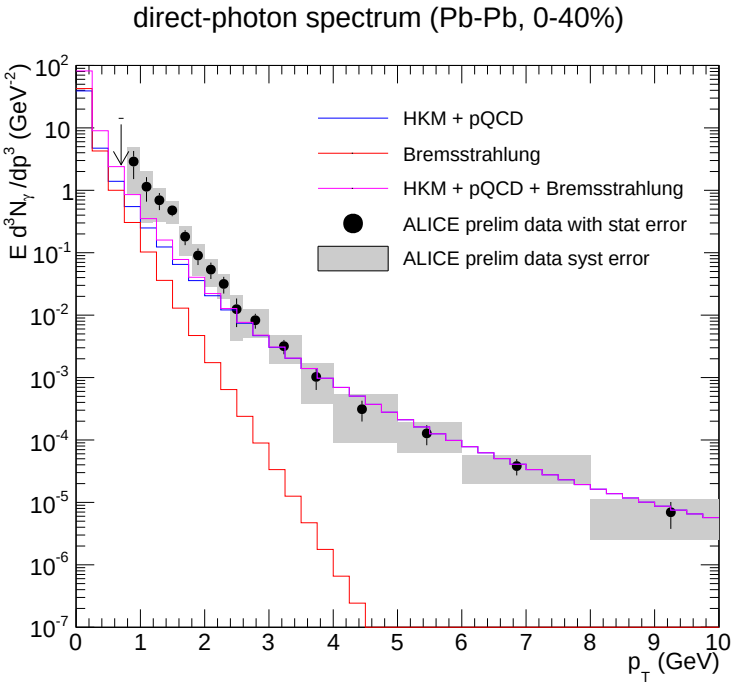

Figure 6.1: Bremsstrahlung correction is no solution of the photon puzzle.

6.2 Pseudo-critical Enhancement

Inspired by a publication of Hees et al. [31] an attempt to solve the photon puzzle with the inclusion of a pseudo-critical enhancement is presented here.

As discussed in detail in that publication the transition region at $T_c \approx 160$MeV is identified as a key contributer to thermal photon spectra. Confining interactions are expected to make an important contribution close to the hadronization transition. There will be an increase in partonic scattering rates and this leads to a natural increase of photon radiation. These photon rates should be higher than those from

interacting particles, calculated in perturbative models.

To decode the photon puzzle, a phenomenological "pseudo-critical enhancement" was taken into account in our calculations. To implement such an enhancement we increased the rates by

$$F(T) = 1 + (f_{max} - 1)\frac{g(T - T_c, \sigma)}{g(0, \sigma)} \tag{6.2}$$

where $g(x, \sigma)$ is the Gaussian distribution. As we can see $F(T_c) = f_{max}$ and $F(T) = 1$ if T is large respectively small compared to T_c. Thus the increase is located in the vicinity of T_c. This ansatz is purely phenomenologically motivated.

The data (photon yield) was not fitted. Trying different f_{max} and σ we got the best result for the photon yield at $f_{max} = 15$ and $\sigma = 0.02$ GeV. To get an impression of the order of magnitude see appendix A.5.

Figure 6.2 and 6.3 show the results. The invariant photon yield at low p_T is significantly increased and all measured data from low to high p_T are well described. As expected, the v_2 spectra has grown due to a later emission stage. The pseudo-critical enhancement seems to be a possible solution for the photon puzzle.

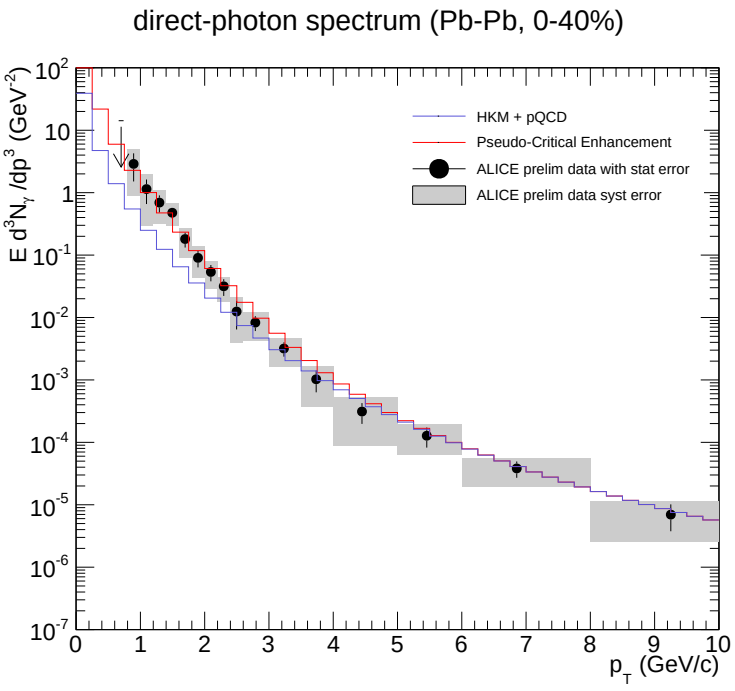

Figure 6.2: The pseudo-critical enhancement provides essential contributions at low p_T.

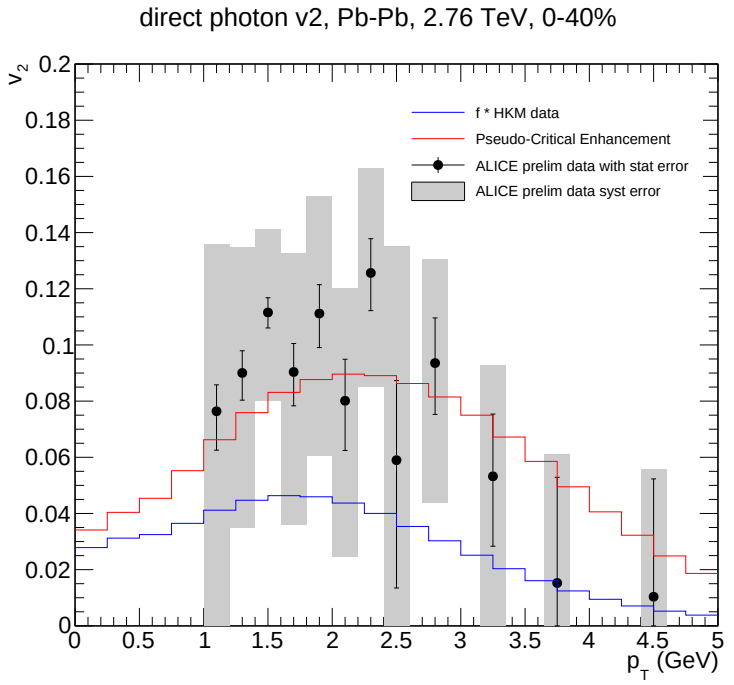

Figure 6.3: The pseudo-critical enhancement provides high v_2-values.

7. Conclusions and Outlook

This thesis deals with the direct photons from the fireball formed in heavy ion collisions. The focus is set on the observables direct photon yield and direct photon elliptic flow v_2. Results are compared to ALICE measurements of lead-lead collisions with a center-of-mass energy of $\sqrt{s_{NN}} = 2.76$ TeV.

The measurements of the direct photon yield show a large T_{slope} for $1 \leq p_T \leq 3$GeV. Although this slope can be interpreted as a signal of a very high temperature of the fireball at an early stage, this does not explain the measured values of v_2. Thus this interpretation can be considered misleading. It was the aim of this thesis to give hints to solve this photon puzzle. The model should describe the direct photon yield and the elliptic flow v_2 simultaneously.

Hydrokinetic Models are able to describe the transverse momentum distribution of hadrons in Pb-Pb-collisions. Therefore it comes to mind to apply this description of the flow to the calculations of direct photon production.

The observables were calculated on the basis of the Hydrokinetic Model [23, 17, 24, 25, 19] with the help of existing parametrizations for the emission of direct thermal photons [26] in the quark gluon plasma (QGP) and an adequate description of the emission of the following hadron gas (HG) [27] . Instead of a soft crossover a hard transition between QGP and HG at a temperature $T_c = 160$ MeV was implemented for the calculation of the photonrates.

The resulting invariant direct photon yield shows a deviation downward from the measurement over the entire range of p_T, especially at low and high p_T. High p_T deviations were solved by adding the pQCD photons using a parametrization by Werner Vogelsang. The amount of the elliptic flow v_2 is not described by this approach. So the photon rates from the space-time evolution from the HKM confirm the above mentioned photon puzzle.

To solve the photon puzzle, additional photon sources from later points of the expansion were included. The inclusion of photons emitted by meson-meson and meson-

baryon bremsstrahlung did not reproduce the measurement at low p_T. It is therefore suggested that bremsstrahlung can only be a part of the solution for the photon puzzle.

Inspired by a recent publication from Hees et al. [31] a phenomenological "pseudo-critical enhancement" was taken into account in the calculations. They have interpreted the transition region as a key contributer to thermal photon spectra. At this stage of the fireball evolution there will be an increase in partonic scattering rates and this leads to a natural increase of photon radiation.

This has been modeled by adding a Gaussian distribution around the critical temperature. Best results gave a 15 times higher photon production at the critical temperature with a standard deviation of $\sigma = 0.02$ GeV.

With this approach the invariant direct photon yield and v_2 are well described simultaneously.

This indicates that the phase transition delivers extra direct photons. Investigations towards a better theoretical/phenomenological understanding of this thermal stage could lead to a better understanding of the evolution of the fireball.

Recently Rapp et al. [34] published a new parametrization for the hadron gas rates (see appendix A.4). The deviation to the old rates is small. It does not give a hint to the photon puzzle.

A. Appendix

A.1 Basic Kinematics

In the first step we introduce the basics of relativistic kinematics. Let

$$x^\mu = (t, x, y, z) \tag{A.1}$$

be the 4-vector and with $g_{\mu\nu} = diag(1, -1, -1, -1)$ and $c = 1$. We define the proper time τ

$$\tau = \sqrt{g_{\mu\nu} x^\mu x^\nu}. \tag{A.2}$$

Now u^μ is defined by:

$$u_\beta \equiv \frac{\partial \tau}{\partial x^\beta} = \frac{1}{2\tau}(g_{\mu\nu} x^\mu \delta^{\beta\nu} + g_{\mu\nu} x^\nu \delta^{\beta\mu}) = \frac{1}{\tau} g_{\mu\beta} x^\mu = \frac{x_\beta}{\tau} \tag{A.3}$$

It is clear that $u_\mu u^\mu = \frac{x_\mu x^\mu}{\tau^2} = 1$ and for later use $\partial_\nu u_\mu u^\mu = 2 u_\mu \partial_\nu u^\mu = 0$.
Now we define $\vec{\beta} \equiv \frac{d\vec{x}}{dt}$. In general the rapidity is defined by:

$$y = \tanh^{-1}(|\vec{\beta}|) = \frac{1}{2} \ln \frac{1 + |\vec{\beta}|}{1 - |\vec{\beta}|} \tag{A.4}$$

Now we assume a particle moving into z-direction, then let the space-time rapidity Y and y the rapidity of a particle with constant velocity located at the origin of the lab frame at time $t = 0$. Then

$$\cosh(Y) \equiv \gamma_z = \frac{1}{\sqrt{1 - \beta_z^2}} = \cosh(y). \tag{A.5}$$

This is equivalent to

$$Y = \frac{1}{2} \ln \frac{1 + \beta_z}{1 - \beta_z} = \frac{1}{2} \ln \frac{E + p_z}{E - p_z} = \frac{1}{2} \ln \frac{t + z}{t - z}. \tag{A.6}$$

In this case $\tau = \sqrt{t^2 - z^2}$. Now any x^μ in this frame can be rewritten as

$$x^\mu = (\tau cosh(Y), r\cos(\phi), r\sin(\phi), \tau\sinh(Y)). \tag{A.7}$$

In this variables d^4x is transformed to

$$d^4x = dtdxdydz = \tau d\tau dY dxdy = \tau d\tau dY r dr d\phi. \tag{A.8}$$

If we define the energy-momentum vector p^μ for particle with mass m_0 by

$$p^\mu = m_0 u^\mu. \tag{A.9}$$

Now let the particle have the rapidity $Y = 0$ in the system S^*. In this system we define $\beta_T \equiv \sqrt{\beta_x^2 + \beta_y^2} = \tanh(\rho)$ or

$$\rho = \frac{1}{2}\ln\frac{1+\beta_T}{1-\beta_T} \tag{A.10}$$

Defining

$$p_T \equiv m_0 \sinh(\rho) \tag{A.11}$$

and

$$m_T \equiv m_0 \cosh(\rho) \tag{A.12}$$

it is $m_0^2 = m_T^2 - p_T^2$ and the energy-momentum vector is now given by

$$p^\mu = (E, p_x, p_y, p_z) = (m_T\cosh(Y), p_T\cos(\phi), p_T\sin(\phi), m_T\sinh(Y)). \tag{A.13}$$

Now, we can rewrite the resulting u^μ as

$$u^\mu = \begin{pmatrix} \cosh(Y)\cosh(\rho) \\ \sinh(\rho)\cos(\varphi) \\ \sinh(\rho)\sin(\varphi) \\ \sinh(Y)\cosh(\rho) \end{pmatrix} = \frac{p^\mu}{m_0} = \frac{m_T}{m_0}\begin{pmatrix} \cosh(Y) \\ \frac{p_T}{m_T}\cos(\varphi) \\ \frac{p_T}{m_T}\sin(\varphi) \\ \sinh(Y) \end{pmatrix}. \tag{A.14}$$

A.2 Basic Relativistic Hydrodynamics and Energy Stress Tensor

The energy stress tensor is defined by

$$T^{\mu\nu} = (\epsilon(x) + p(x))u(x)^{\mu}u(x)^{\nu} - g^{\mu\nu}p(x) \tag{A.15}$$

where in the case of hydrodynamics $\epsilon(x)$ is the energy density and $p(x)$ is the pressure. Energy-momentum conservation is expressed

$$\partial_{\mu}T^{\mu\nu} = 0. \tag{A.16}$$

Now we get 4 equations:

$$0 = \partial_{\mu}T^{\mu\nu} = (\epsilon + p)u^{\mu}\partial_{\mu}u^{\nu} + u^{\nu}\partial_{\mu}(\epsilon + p)u^{\mu} - g^{\mu\nu}\partial_{\mu}p \tag{A.17}$$

Multiplying by u_{ν} we get:

$$0 = u_{\nu}\partial_{\mu}T^{\mu\nu} = (\epsilon + p)u^{\mu}u_{\nu}\partial_{\mu}u^{\nu} + u_{\nu}u^{\nu}\partial_{\mu}(\epsilon + p)u^{\mu} - u_{\nu}g^{\mu\nu}\partial_{\mu}p \tag{A.18}$$

Using $u_{\nu}\partial_{\mu}u^{\nu} = 0$, this leads to:

$$u^{\mu}\partial_{\mu}\epsilon = -(\epsilon + p)\partial_{\mu}u^{\mu}. \tag{A.19}$$

This is one equation. To get the other three equations, we have to multiply $\partial_{\mu}T^{\mu\nu} = 0$ by factor $(g_{\alpha\nu} - u_{\alpha}u_{\nu})$

$$0 = (g_{\alpha\nu} - u_{\alpha}u_{\nu})[(\epsilon + p)u^{\mu}\partial_{\mu}u^{\nu} + u^{\nu}\partial_{\mu}(\epsilon + p)u^{\mu} - g^{\mu\nu}\partial_{\mu}p] \tag{A.20}$$

which results into

$$0 = (\epsilon + p)u^{\mu}\partial_{\mu}u_{\alpha} + u_{\alpha}\partial_{\mu}(\epsilon + p)u^{\mu} - \partial_{\alpha}p - u_{\alpha}\partial_{\mu}(\epsilon + p)u^{\mu} + u_{\alpha}u^{\mu}\partial_{\mu}p \tag{A.21}$$

and finally

$$0 = -\partial_{\alpha}p + u_{\alpha}u^{\mu}\partial_{\mu}p + (\epsilon + p)u^{\mu}\partial_{\mu}u_{\alpha}. \tag{A.22}$$

The hydrodynamic phase is now described by:

$$u^{\mu}\partial_{\mu}\epsilon = -(\epsilon + p)\partial_{\mu}u^{\mu} \tag{A.23}$$

and the Euler equation

$$0 = -\partial_\alpha p + u_\alpha u^\mu \partial_\mu p + (\epsilon + p) u^\mu \partial_\mu u_\alpha. \tag{A.24}$$

(A.23) and (A.24) represent four independent equations.

A.3 Thermodynamics

To solve (A.23) and (A.24) more information is needed. In the hydrodynamic description this information is given by the equation of state (EOS). We are interested in the intensive properties of the QGP.

$$\epsilon + p = Ts + \mu n \tag{A.25}$$

and

$$dp = sdT + nd\mu \tag{A.26}$$

where ϵ an p are the energy density and the pressure. T is the temperature, μ the chemical potential, s the entropy density and n the particle density. With

$$d\epsilon = -dp + Tds + sdT + \mu dn + nd\mu = Tds + \mu dn \tag{A.27}$$

equation (A.25), (A.26) and (A.27) are the basic framework to calculate the hydrodynamic expansion. Together with

$$\partial_\nu s u^\nu = 0 \tag{A.28}$$

which follows from $\partial_\mu n u^\mu = 0$, we have enough information to calculate special cases of the equation of state.
As an example the energy density of an ideal relativistic gas is calculated:

$$\epsilon(\beta) = \frac{E(\beta)}{V} = g\frac{4\pi}{(2\pi\hbar)^3}\int_0^\infty p^2 E(p)\frac{1}{e^{\beta E(p)} \pm 1}dp \tag{A.29}$$

where g is the the degree of freedom, $\beta = 1/T$ and the "-" is for bosons and the "+" for fermions. In the case of bosons, we calculate

$$\epsilon(\beta) = g\frac{4\pi}{(2\pi\hbar)^3}\int_0^\infty p^3\frac{1}{e^{\beta p} - 1}dp = g\frac{4\pi}{(2\pi\hbar)^3}\frac{1}{\beta^4}\int_0^\infty x^3\frac{1}{e^x - 1}dx = g\frac{3}{\pi^2\hbar^3}T^4\frac{\pi^4}{90}. \tag{A.30}$$

In the case of fermions the same calculation leads to:

$$\epsilon(\beta) = g\frac{3}{\pi^2\hbar^3}T^4\frac{\pi^4}{90}\frac{7}{8} \tag{A.31}$$

(A.31) shows the typical T^4-behavior of the energy density of the QGP.
To calculate the pressure, we have to recall, that $P_x = P_y = P_z$ and $P_x =< \frac{p_x v_x}{V} >$. While $P_{x,y,z} = \frac{1}{3V}(p_x v_x + p_y v_y + p_z v_z)$, we conclude

$$P = \frac{1}{3V}\vec{p}\vec{v} = \frac{1}{3V}\vec{p}\frac{\vec{p}}{E} = \frac{1}{3V}\frac{p^2}{E} = \frac{1}{3V}\frac{p^2 + m^2 - m^2}{E} = \frac{1}{3V}(E - \frac{m^2}{E}) \qquad \text{(A.32)}$$

[here P is the pressure]. In the ultrarelativistic case ($m \approx 0$) the pressure is $p = \frac{\epsilon}{3}$.

A.4 New Parametrization for the Thermal Photon Rates from the HG

A recent publication by Rapp et.al [34] shows a new universal parametrization for the photon emission rates from the hadron gas. These rates include the contribution from in-medium ρ mesons, as well as bremsstrahlung from $\pi\pi$ scattering.

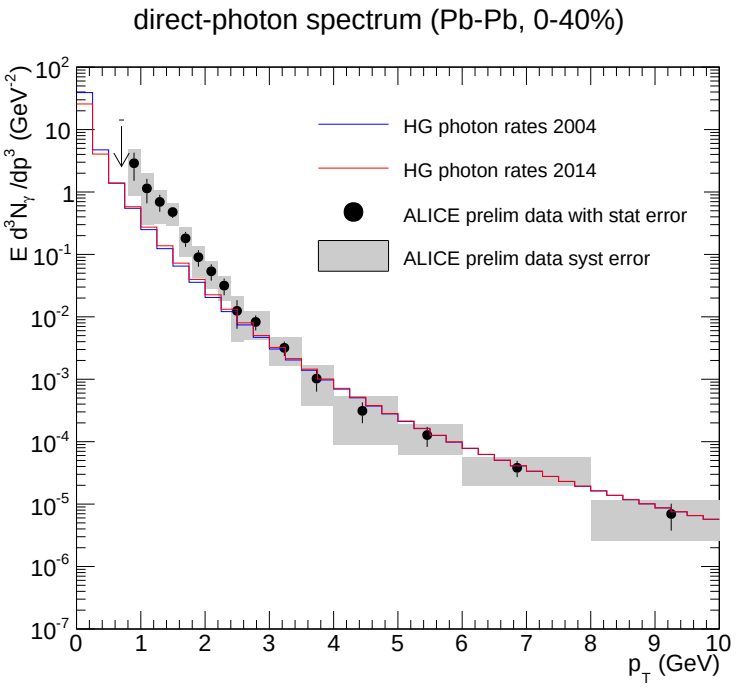

Figure A.1: Photons from the HKM and qQCD photons. The new parametrization of the hadron gas rates only gives rise to a small increase of the photon yield at low p_T. This does not give a hint to the solution of the photon puzzle.

A comparison of the invariant photon yield calculated with the new rates and the invariant photon yield from the old rates is shown in figure A.1. We obtain only a small deviation. A small increase of the yield at low p_T can be seen. Although the deviation effects the questionable region, it seems to be negligible for our problem and it can not explain the photon puzzle.

A.5 Pseudo-Critical Enhancement - Impact of f_{max} and σ

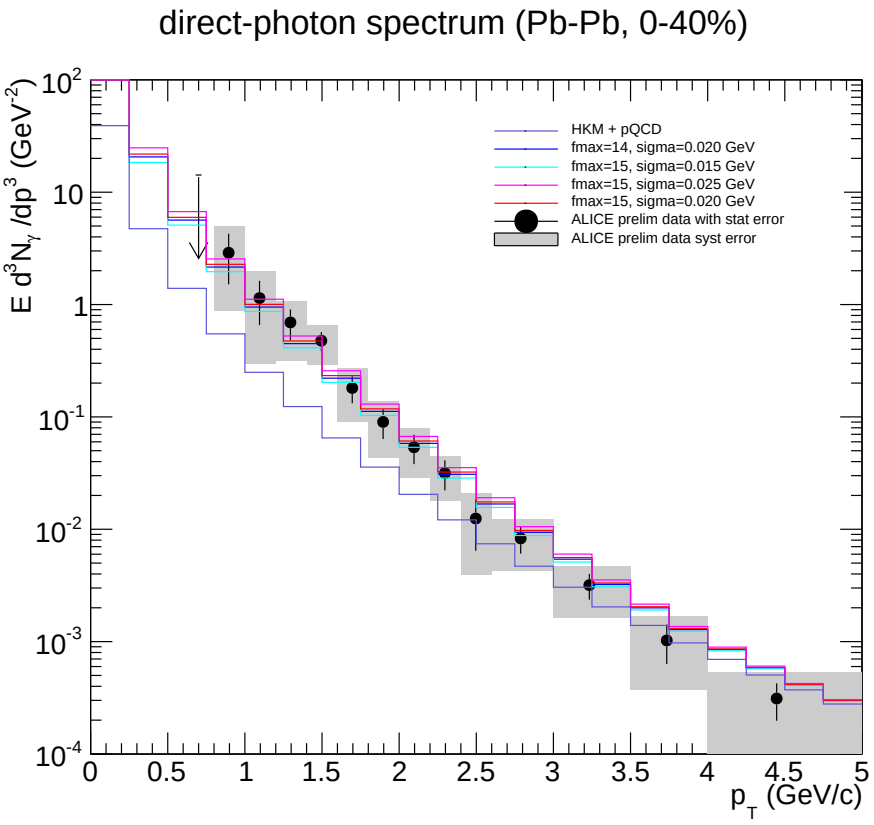

Figure A.2: To get an impression of the order of magnitude of f_{max} and σ here photon yields with values close to the chosen ones are given.

Bibliography

[1] Rene Brun and Fons Rademakers. ROOT - An Object Oriented Data Analysis Framework, Proceedings AIHENP'96 Workshop, Lausanne, Sep. 1996, Nucl. Inst. & Meth. in Phys. Res. A 389 (1997) 81-86. See also http://root.cern.ch/., 1997.

[2] Alice Collaboration, F Carminati, P Foka, P Giubellino, A Morsch, G Paic, J-P Revol, K Safarík, Y Schutz, and U A Wiedemann (editors). ALICE: Physics Performance Report, Volume I. *Journal of Physics G: Nuclear and Particle Physics*, 30(11):1517–1763, November 2004.

[3] Peter Braun-Munzinger and Johanna Stachel. The quest for the quark–gluon plasma. *Nature*, 448(7151):302–309, July 2007.

[4] K.A. Olive. Review of particle physics. *Chinese Physics C*, 38(9):090001, 2014.

[5] D. Lohner. Measurement of Direct-Photon Elliptic Flow in Pb-Pb Collisions at $\sqrt{s_{NN}} = 2.76$ TeV. *arXiv:1212.3995*, 2013.

[6] Adare et. al. Observation of Direct-Photon Collective Flow in Au+Au Collisions at $\sqrt{s_{NN}} = 200$ GeV. *Physical Review Letters*, 109, September 2012.

[7] R.J. Fries and B. Müller. Heavy ions at LHC: Theoretical issues. *The European Physical Journal C*, 34(S1):s279–s285, July 2004.

[8] R. Stock. Relativistic Nucleus-Nucleus Collisions and the QCD Matter Phase Diagram. *arXiv:0807.1610*, 2008.

[9] Akitomo Enokizono. Space-time evolution of hot and dense matter probed by Bose-Einstein correlation in Au+Au collisions at $\sqrt{s_{NN}} = 200$ GeV. *http://inspirehep.net/record/673843/*, 2004.

[10] J. D. Bjorken. Highly relativistic nucleus-nucleus collisions: The central rapidity region. *Physical Review D*, 27(1):140–151, January 1983.

[11] S. V. Akkelin and Yu. M. Sinyukov. Matching of nonthermal initial conditions and hydrodynamic stage in ultrarelativistic heavy-ion collisions. *Physical Review C*, 81(6), June 2010.

[12] Paul Stankus. Direct photon production in relativistic heavy-ion collisions. *Annual Review of Nuclear and Particle Science*, 55(1):517–554, December 2005.

[13] Kohsuke. Yagi, Tetsuo. Hatsuda, and Yasuo. Miake. *Quark-gluon plasma: from Big Bang to Little Bang*. Cambridge University Press, Cambridge; New York, 2008.

[14] Raimond Snellings. Elliptic flow: a brief review. *New Journal of Physics*, 13(5):055008, May 2011.

[15] Daniel Lohner. Anisotropic flow of direct photons in Pb-Pb collisions at 2.76 TeV per nucleon. *urn:nbn:de:bsz:16-heidok-156507*, October 2013.

[16] B. Abelev et. al. Pion, Kaon, and Proton Production in Central Pb-Pb Collisions at $\sqrt{s_{NN}} = 2.76TeV$. *Physical Review Letters*, 109(25), December 2012.

[17] S. Akkelin, Y. Hama, Iu. Karpenko, and Yu. Sinyukov. Hydro-kinetic approach to relativistic heavy ion collisions. *Physical Review C*, 78(3), September 2008.

[18] Yu A Karpenko and Yu M Sinyukov. Femtoscopic scales in central A+A collisions at RHIC and LHC energies in a hydrokinetic model. *Journal of Physics G: Nuclear and Particle Physics*, 38(12):124059, December 2011.

[19] Iu. Karpenko, Yu. Sinyukov, and K. Werner. Uniform description of bulk observables in the hydrokinetic model of collisions at the BNL Relativistic Heavy Ion Collider and the CERN Large Hadron Collider. *Physical Review C*, 87(2), February 2013.

[20] Jean-Yves Ollitrault. Relativistic hydrodynamics for heavy-ion collisions. *European Journal of Physics*, 29(2):275–302, March 2008.

[21] Y. Sinyukov , Kiev. Spatiotemporal picture of relativistic nucleus-nucleus collisions @ EMMI Meeting 27.2.2014 , 2014.

[22] S. V. Akkelin and Yu. M. Sinyukov. Entanglement of scales as a possible mechanism for decoherence and thermalization in relativistic heavy ion collisions. *Physical Review C*, 89(3), March 2014.

[23] Yu. Sinyukov, S. Akkelin, and Y. Hama. Freeze-Out Problem in Hydrokinetic Approach to A+A Collisions. *Physical Review Letters*, 89(5), July 2002.

[24] Iu. A. Karpenko and Yu. M. Sinyukov. Kaon and pion femtoscopy at the highest energies available at the BNL Relativistic Heavy Ion Collider RHIC in a hydrokinetic model. *Physical Review C*, 81(5), May 2010.

[25] Iu.A. Karpenko and Yu.M. Sinyukov. Energy dependence of pion interferometry scales in ultra-relativistic heavy ion collisions. *Physics Letters B*, 688(1):50–54, April 2010.

[26] Peter Arnold, Guy D Moore, and Laurence G Yaffe. Photon emission from quark-gluon plasma: complete leading order results. *Journal of High Energy Physics*, 2001(12):009–009, December 2001.

[27] Simon Turbide, Ralf Rapp, and Charles Gale. Hadronic production of thermal photons. *Physical Review C*, 69(1), January 2004.

[28] Ekkard Schnedermann, Josef Sollfrank, and Ulrich Heinz. Thermal phenomenology of hadrons from 200A GeV S+S collisions. *Physical Review C*, 48(5):2462–2475, November 1993.

[29] W. Vogelsang. private communication, 2014.

[30] B. Abelev et. al. Neutral pion production at midrapidity in pp and Pb–Pb collisions at $\sqrt{s_{NN}}$=2.76 TeV. *The European Physical Journal C*, 74(10), October 2014.

[31] Hendrik van Hees, Min He, and Ralf Rapp. Pseudo-critical enhancement of thermal photons in relativistic heavy-ion collisions? *Nuclear Physics A*, September 2014.

[32] O. Linnyk, W. Cassing, and E. L. Bratkovskaya. Centrality dependence of the direct photon yield and elliptic flow in heavy-ion collisions at $\sqrt{s_{NN}} = 400$ GeV. *Physical Review C*, 89(3), March 2014.

[33] O. Linnyk. private communication, 2014.

[34] Matthew Heffernan, Paul Hohler, Ralf Rapp. Universal Parametrization of Thermal Photon Rates in Hadronic Matter. *http://arxiv.org/abs/1411.7012*, November 2014.

Acknowledgement

First of all, I would like to thank my supervisor PD Dr. Klaus Reygers, for the opportunity to carry out my bachelor thesis in his group and to become involved in the ALICE experiment. I took great benefits from his help and guidance. Secondly I would like to thank Prof. Dr. Norbert Herrmann for reading and evaluating my thesis.

Special thanks go to Yuri Sinyukov, Werner Vogelsang and Olena Linnyk for providing results of their calculations used in this thesis.

I want to thank the ALICE group for giving me the opportunity to present and discuss my results in the group meeting and especially Dr. Michael Knichel and Michael Schork for proofreading my thesis.

I greatly appreciate the time Bernd Epding and my sister Ulrike spend for proofreading this thesis.

Finally, I wish to express my gratitude to my parents for their constant support of my studies.